Chalcogenide Letters Vol. 21, No.8, August 2024, p. 615 - 629

A first-principles investigation of Ba_2CaTeO_6 and Ba_2CaWO_6 compounds for thermoelectric and optoelectronic applications

M. Ishfaq[a], A. Aziz[a], S. A. Aldaghfag[b], S. Noreen[c], M. Zahid[c], M. Yaseen[a,*]
[a]*Spin-Optoelectronics and Ferro-Thermoelectric (SOFT) Materials and Devices Laboratory, Department of Physics, University of Agriculture, Faisalabad 38040, Pakistan*
[b]*Department of Physics, College of Sciences, Princess Nourah bint Abdulrahman University, P. O. Box 84428, Riyadh 11671, Saudi Arabia*
[c]*Department of Chemistry, University of Agriculture Faisalabad, Faisalabad 38040, Pakistan*

Herein, structural, optoelectronic, and thermoelectric characteristics of Ba_2CaTeO_6 and Ba_2CaWO_6 oxides double perovskite have been evaluated by first-principles calculations. Enthalpy of formation and tolerance factor are computed to ensure the respective structural and thermodynamical stability. Ba_2CaTeO_6 and Ba_2CaWO_6 have mBJ computed bandgaps of 5.87 eV and 4.20 eV, respectively. Furthermore, the optical parameters like dielectric constants ($\varepsilon_1(\omega)$ & $\varepsilon_2(\omega)$) and other related parameters are computed. The thermoelectric (TE) parameters were examined using the BoltzTraP package. The ZT values of $Ba_2Ca(Te/W)O_6$ at 450 K are 0.76/0.79, respectively. The outcomes of the Ba_2CaTeO_6 and Ba_2CaWO_6 double perovskite show that these materials are potential contenders for UV-based optical and various TE gadgets.

(Received May 12, 2024; August 5, 2024)

Keywords: Ultrawide bandgap semiconductors, Double perovskites, DFT, Thermoelectrics, Optoelectronics

1. Introduction

Traditional semiconductor materials with electronic bandgaps (E_g) of less than 2.3 eV, like Si, Ge, and III-V compounds have served as the foundation for technical advancements in electronics and photonics. On the other hand, semiconductors with E_g greater than 3.4 eV are referred to as ultrawide bandgap (UWBG) semiconductors [1-3]. For instance, GaN – an UWBG semiconductor, has overtaken Si as the second most important material in the previous 15 years, because of its use in solid-state lighting, which has drastically altered the way of world uses light sources. However, high fabrication cost of GaN, coupled with its poor hole mobility and low thermal conductivity, restrict its implications in electronic industry at full scale [4]. In this regard, scientists are putting forth significant efforts in the quest to develop the alternative UWBG materials. Recently, double perovskites (DPs) have emerged as standalone family of compounds which show diverse and fascinating characteristics from half metallic to narrow bandgap to ultrawide bandgap semiconducting properties owing to their ability to host wide variety of cations in ideally cubic (Fm3m space group) lattice structure [5-7].

The general formula of oxide double perovskites is $A_2BB'O_6$ which shows stability in orthorhombic, cubic, monoclinic, or tetragonal phase depending upon the selection of cations. The B site cationic ordering has been regarded as major factor which influences the physical properties of DPs [8]. Various studies have shown the dependence of the characteristics of DPs on the cationic combination. Besbes and co-workers used the first-principles method to investigate thermoelectric (TE) and magnetic characteristics of Ba_2CeCoO_6 oxide and revealed the half-metallic ferromagnetic (HMF) characteristics with figure of merit (ZT) value of 0.94 at 300 K [9]. Amaria et al. analyzed Pb_2FeTaO_6 for optoelectronic devices and reported the ZT (0.95) at 300 K [10]. Samah Al-Qaisi et al. examined Ba_2NaIO_6 for infrared optoelectronic devices and determined

* Corresponding author: myaseen_taha@yahoo.com
https://doi.org/10.15251/CL.2024.218.615

the ZT value of 0.78 [11]. Brik explored electronic features of cubic Ba_2MgWO_6 double perovskite by using ab-initio approach and found the indirect bandgap of 2.89 eV [12]. Musa et al. utilized first principles computations to examine the electro-magnetic features of Ba_2ATaO_6 (A = Mn, Fe, Cr) and predicted an insulating behavior of Ba_2FeTaO_6 and Ba_2CrTaO_6 while Ba_2MnTaO_6 exhibit HMF with 3.98 μ_B [13]. Saad H-E and Rammeh examined the electro-magnetic characteristics of Ba_2FeWO_6 through an experimental and theoretical study. The characteristics of the Ba_2FeWO_6 compound was found that it undergoes to paramagnetic from antiferromagnetic phase at T_N=20 K [14]. Hansraj et al. performed DFT calculations to explore thermoelectric and optical features of Ba_2SbTaO_6 and Ba_2SbNbO_6 [15]. Ghebouli et al. explored physical characteristics of Sr_2AlMO_6 (M=Ta, Nb, V) by ab initio method. Sr_2AlTaO_6 and Sr_2AlNbO_6 revealed the direct E_g, while Sr_2AlVO_6 expressed an indirect E_g [16]. Haid et al. investigated the Ba_2HoReO_6 theoretically and discovered that it had an indirect E_g of 0.32 eV with 6.0 μ_B [17]. Sajad Ahmad Dar et al. studied the physical features of Ba_2InTaO_6 and the highest power factor with a value of 1.20 $\times 10^{12}$ W/mK^2s at 1000 K [18]. Comprehensive literature review suggests that DPs are important family of compounds having potential for their applications in advanced technological applications [19-27].

Specifically, $Ba_2Ca(Te/W)O_6$ are needed to be explored computationally. Both mentioned materials have been experimentally synthesized previously reporting their stable cubic structures [28, 29]. An experimental study on Ba_2CaWO_6 revealed that a small amount of oxygen deficiency hugely distorts its cubic structure [30]. Various other experimental and theoretical studies on Ba_2CaWO_6 and Ba_2CaTeO_6 have been reported and incorporation of another cation in its cubic structure was regarded as effective way to tune its photonic properties [31–49]. In this paper, we consider two DPs Ba_2CaXO_6 (X = Te, W) to computationally investigate the physical properties including structural, optoelectronic, and thermoelectric (TE) characteristics. Until now, there is not any computational study available in literature on mentioned DPs which prompted us to consider these materials for comprehensive theoretical investigation based on density functional theory (DFT). Both Ba_2CaXO_6 (X = Te, W) are found to have stable cubic structure along with superior optical absorption and high thermoelectric figure of merit (ZT) which imply their importance for possible applications in advanced technologies including optical sensors, TE coolers, and energy storage devices.

2. Computational details

Thermoelectric and optoelectronic characteristics of Ba_2CaXO_6 (X = Te, W) compounds have been investigated by employing full-potential linearized augmented plane-wave approach (FP-LAPW) [50] based on DFT as executed in WIEN2k code [51, 52]. The modeled cubic structures of titled DPs go through a division process in FP-LAPW technique and are separated into two regions, the interstitial region and the non-overlapping muffin-tin (MT) section [53–55]. The input data for structural modeling was taken from experimental reports published prior to this work [28, 29]. The modeled structures were further optimized to obtain the ground state phase and parameters. Rest of the calculations was carried out using the optimized cells. For the better estimation of exchange and correlation energies, the generalized gradient approximation (GGA) along with modified Becke Johnson potential was employed [56]. In first Brillouin zone (BZ), 10×10×10 k-points were used for a precise calculation. Plane wave was evaluated by $R_{MT}\times K_{MX}$, the R_{MT} values for the elements in the Ba_2CaXO_6 (X = Te, W) are listed in Table 1. Angular momentum growth in the muffin-tin sphere is taken up to l_{max} = 10 and G_{max} was set at 12 as the maximum Fourier expansion of charge density [57]. The electronic configuration of Ba, Ca, Te, W, and O were set as ($5s^25p^66s^2$), ($4s^2$), ($4d^{10}5s^25p^4$), ($6s^24f^{14}5d^4$), and ($2s^22p^4$), respectively. Self-consistency was obtained with energy convergence near to 10^{-5} Ry. For TE parameter calculations, rigid band approximation and constant relaxation time approximation (CRTA) with $\tau = 10^{-14}$ s was used within BoltzTraP code.

Table 1. The R_{MT} values for Ba_2CaXO_6 (X= Te, W) double perovskite oxides.

Ba_2CaXO_6	X= Te	X= W
Ba	2.5000	2.5000
Ca	2.0500	2.0500
X	1.7500	1.8500
O	1.7500	1.4600

3. Results and discussions

3.1. Structural characteristics

Ba_2CaXO_6 (X = Te, W) have space group Fm3m and crystallize in cubic structures. By using Murnaghan's equation of state (EOS) and volume optimization technique, structural parameters of Ba_2CaTeO_6 and Ba_2CaWO_6 are determined. In Ba_2CaXO_6, the Ba cation in the unit cells of both compounds is situated at (0.25, 0.25, 0.25), the Ca and X anions are at (0, 0, 0) and (0.5, 0.5, 0.5), correspondingly, while the O anions is at (0.2690, 0, 0) Wyckoff position [53]. DFT calculations, as implemented in the WIEN2k program, were utilized to find ground state parameters such as formation energy, lattice parameters, tolerance factor, pressure derivative, Ground state energy (Ry), and bulk modulus (see Table 2).

Table 2. Various determined values for Ba_2CaXO_6(X= Te, W).

Parameters	Ba_2CaTeO_6		Ba_2CaWO_6	
	Current work	Previous	Current work	Previous
Lattice constant Å	8.39	8.3536 [28]	8.36	8.392 [29]
ΔH_f	-3.604		-4.271	
B'	10.7605		7.5330	
Bulk modulus (GPa)	155.7231		164.6055	
Volume (a.u)^3	995.9406		988.4430	
Tolerance factor (τ)	0.93		0.93	
Ground state energy (Ry)	-48392.670288		-67127.986267	

To assure the stability of the compounds, Goldschmidt's tolerance factor (τ_G) [58] has been calculated by using following formula.

$$\tau_G = \frac{\sqrt{2}(r_A + r_O)}{(r_B + r_{B'} + 2r_O)} \quad (1)$$

The τ_G for Ba_2CaTeO_6 and Ba_2CaWO_6 were calculated to be 0.93Å, indicating that investigated materials are stable in the cubic geometry because 0.90-1.05 Å is the stable range for cubic double-perovskite [59, 60]. The optimization curves for both double perovskites offer the lowest energy in the NM (non-magnetic) phase, as illustrated in Fig. 1 (a&c), suggesting that Ba_2CaTeO_6 and Ba_2CaWO_6 are stable in the NM state. Fig. 1 (b&d) depict the stable cubic structures of Ba_2CaTeO_6 and Ba_2CaWO_6, respectively. Enthalpy of formation (ΔH_f) was used for the thermodynamic stability of compounds [61].

$$\Delta H_f = E_{total} - 2E_{Ba} - E_{Ca} - E_{X=Te,W} - 6E_O \quad (2)$$

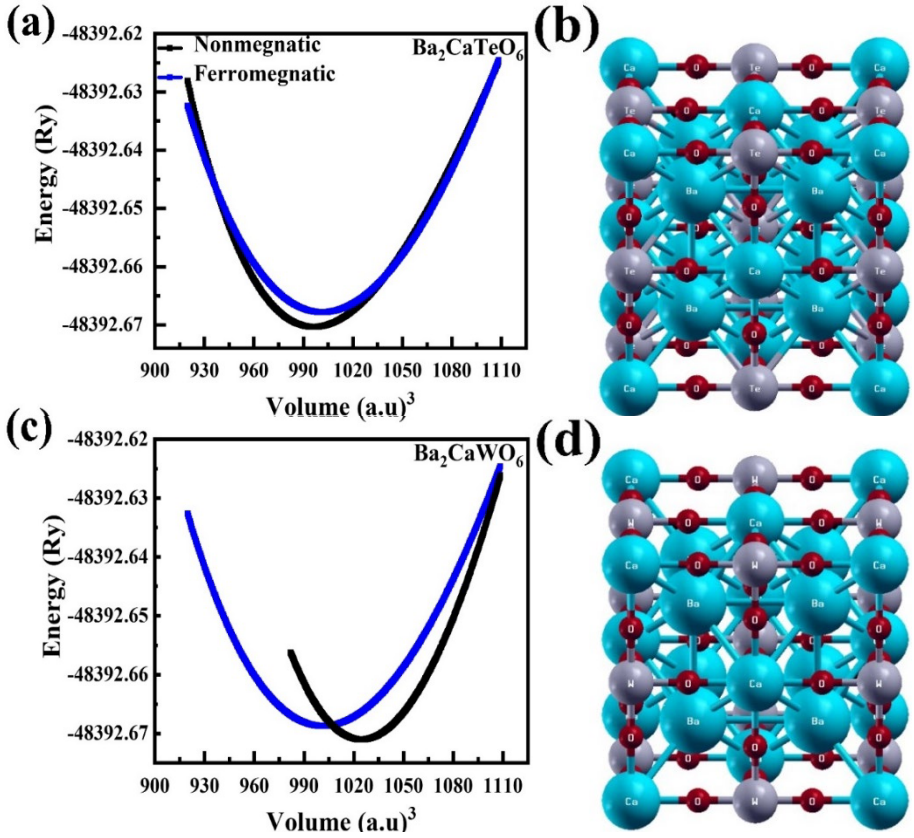

Fig. 1. (a) E-V optimization curve, and (b) Crystal structural of Ba_2CaTeO_6 (c) E-V optimization curve, and (d) Crystal structural of Ba_2CaWO_6.

The total energy of Ba_2CaXO_6 (X = Te, W) double perovskite oxides is given by E_{total}. Computed value of ΔH_f for Ba_2CaTeO_6 is -3.604 eV while for Ba_2CaWO_6 is -4.271 eV, indicating the stability for both DPs. In addition, various experimental studies are available in literature which suggests the thermal stability in functioning environment [39].

3.2. Electronics properties

The electronic structures of double perovskites are probed by computing density of states (DOS) and band structure (BS) [62]. In first BZ, the BS is predicted in a highly symmetric W-L-Γ-X-W-K direction within -8 to 8 eV energy range. Ba_2CaTeO_6 displays a direct wide bandgap of 5.87 eV (see Fig. 2 (a)) at Γ-points and the computed bandgap value of Ba_2CaWO_6 is 4.20 eV (see Fig. 2 (b)).

Valence band maxima show flatness in Γ-X direction. This flatness indicates the degeneracy in between direct and indirect transitions specifically in the case of Ba_2CaWO_6 effect of which is highlighted in Optical Characteristics Section. Total (T) and partial (P) density of states DOS are determined to examine electronic BS deeply [62, 63].

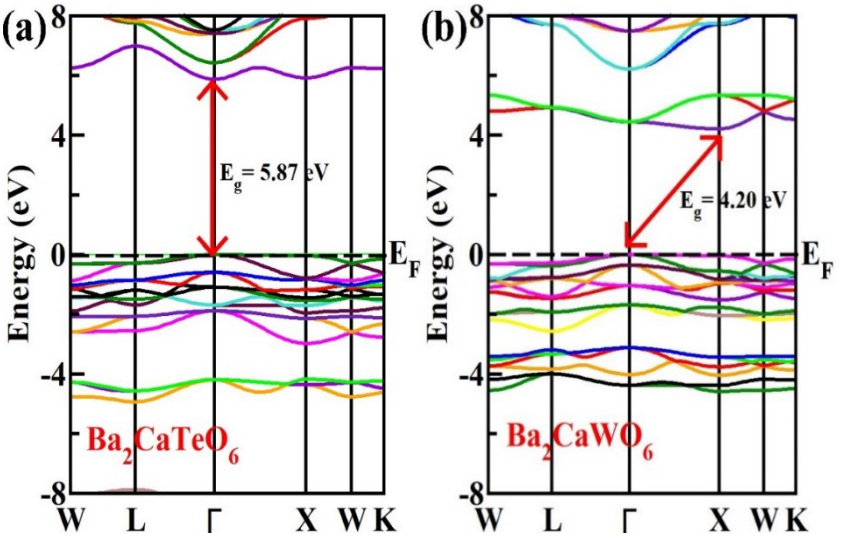

Fig. 2. Computed band structure of Ba_2CaXO_6 (X= Te, W) oxides based double perovskite.

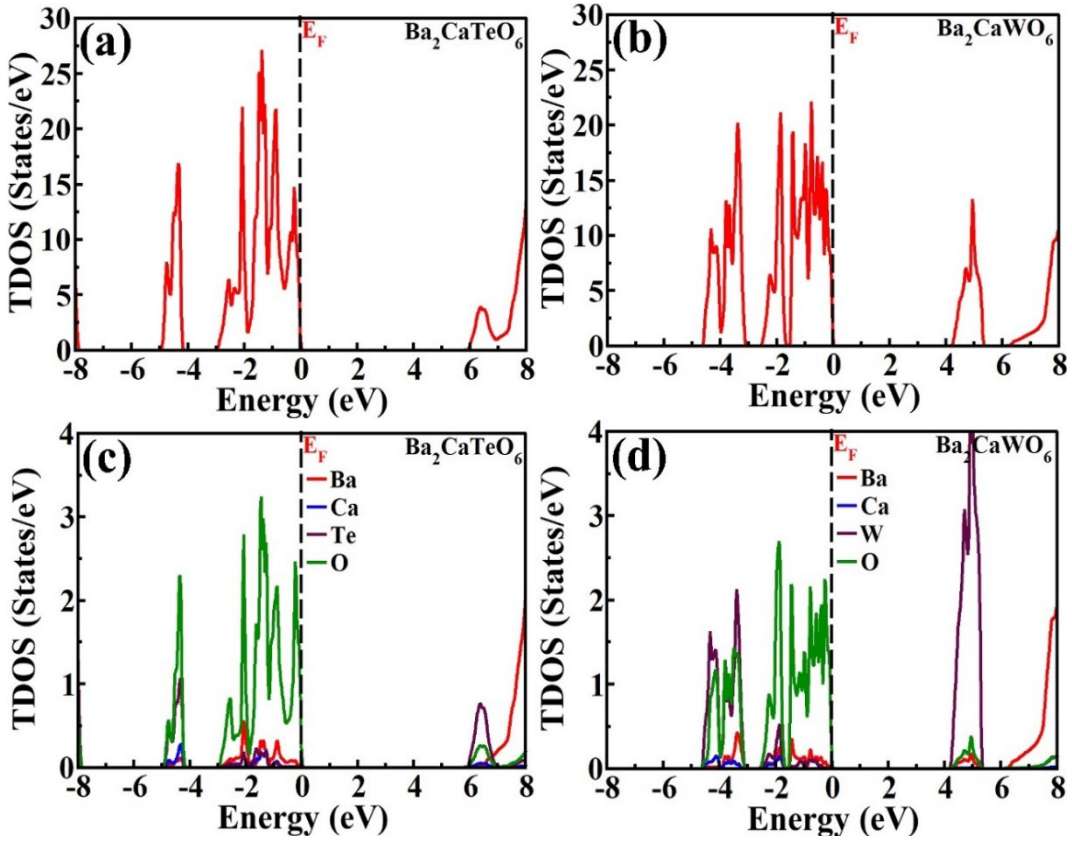

Fig. 3. DOS (a) Ba_2CaTeO_6, (b) Ba_2CaWO_6, and TDOS (c) Ba_2CaTeO_6, (d) Ba_2CaWO_6.

The DOS plots are reflecting well the BS pattern (see Figs. 2 & 3). In the top of VB, only O-atom is contributing strongly (see Fig. 3(c & d)) in the DOS of Ba_2CaXO_6 (X = Te, W) compounds which can be considered as the main source of flatness as shown in BS. While the lower conduction band (CB) is mainly influenced by respective Te/W cations. Sharp peaks (O-*2p* states) were obtained near the E_F from 0 to -3 eV in the VB of Ba_2CaTeO_6, and in this energy range, Ba, Ca, and Te atomic states also have the influenced. The contribution of Te-*s*, O-*2p*, and Ba-*d* state atoms in CB is exhibited in Fig. 4. In the VB of Ba_2CaWO_6, strong peaks of O-*2p* states

were found near the E_F from 0 to -2.5 eV, and in this energy span Ba-*5p*, Ca-*3p*, and W-*5d* states of atoms are also participated. As illustrated in Fig. 5, a prominent peak of the W-*5d* state was observed in CB between 4.16 and 5.35 eV.

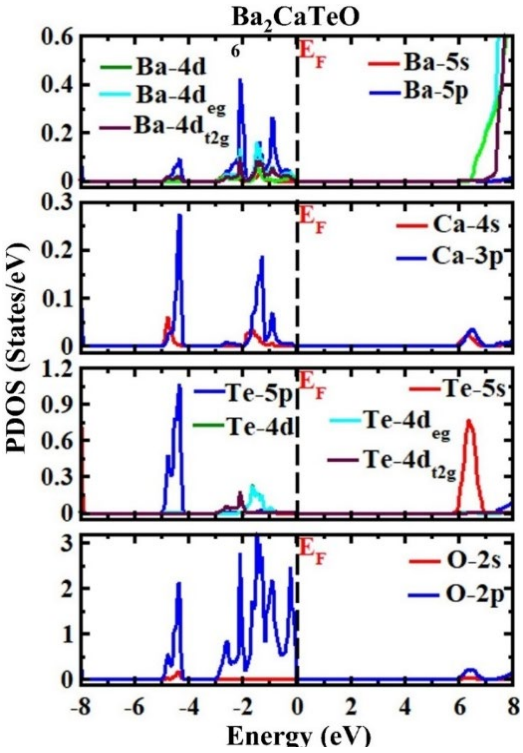

Fig. 4. PDOS for Ba_2CaTeO_6.

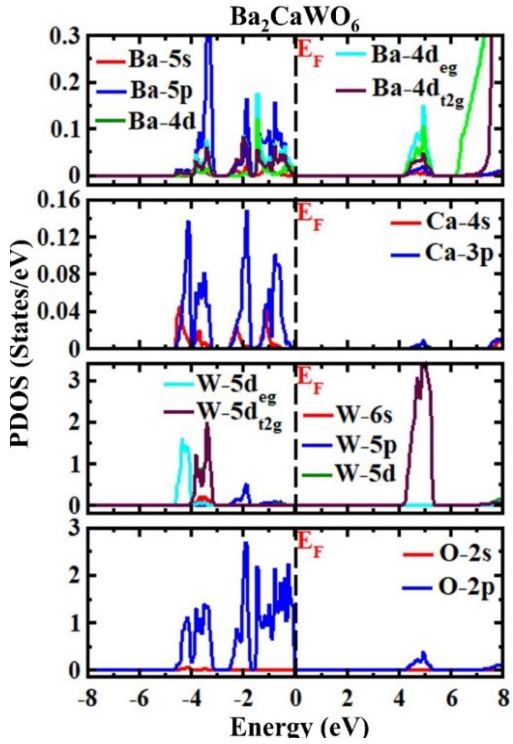

Fig. 4. PDOS for Ba_2CaWO_6.

3.3. Optical characteristics

The optical properties of Ba_2CaTeO_6 and Ba_2CaWO_6 have been investigated for the potential application of investigated compounds in optoelectronic devices. In optical features, the complex dielectric function $\varepsilon(\omega) = \varepsilon_1(\omega) + i\varepsilon_2(\omega)$ is computed to investigate the optical transition between occupied and unoccupied orbitals [64]. $\varepsilon_2(\omega)$ described the absorptive behavior, which is connected to the BS [65]. The Kramers–Kronig relationship [66] can be employed to compute the real $\varepsilon_1(\omega)$ component which defines light polarization.

$$\varepsilon_1(\omega) = 1 + \frac{2}{\pi} P \int_0^{\infty} \frac{\varepsilon_2(\alpha)\alpha d\alpha}{\alpha^2 - \omega^2} \quad (3)$$

Here, P indicates the principal integral value.

For the double perovskites Ba_2CaTeO_6 and Ba_2CaWO_6, all optical parameters were computed and plotted against energy within 0-12 eV. The static dielectric constants $\varepsilon_1(0)$ obtained for Ba_2CaTeO_6 and Ba_2CaWO_6 are 3.30 and 3.96, respectively, and $\varepsilon_1(\omega)$ reaches to its corresponding maximum peak of 5.94/7.57 at 7.03/5.39 eV, respectively (see Fig. 6(a)). The transitions of electrons from VB to CB are reflected by $\varepsilon_2(\omega)$ spectrum.

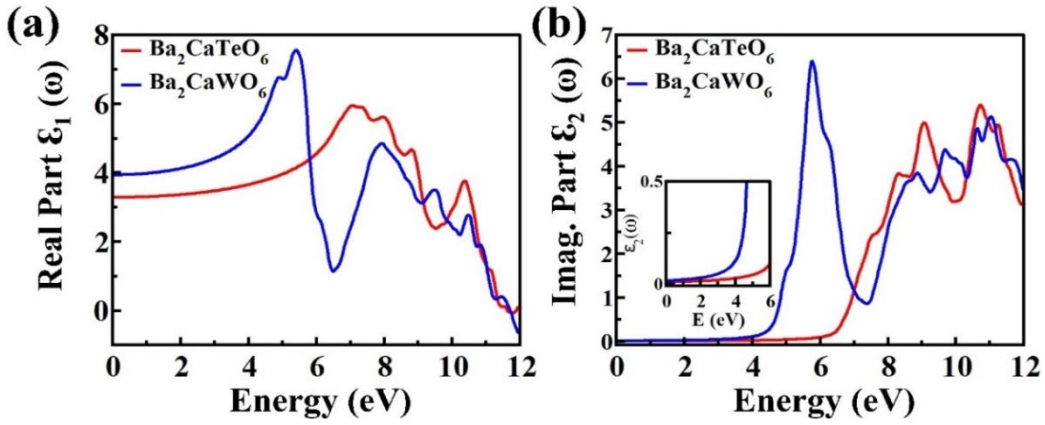

Fig. 6. (a) $\varepsilon_1(\omega)$, (b) $\varepsilon_2(\omega)$ for cubic Ba_2CaXO_6 (X= Te, W).

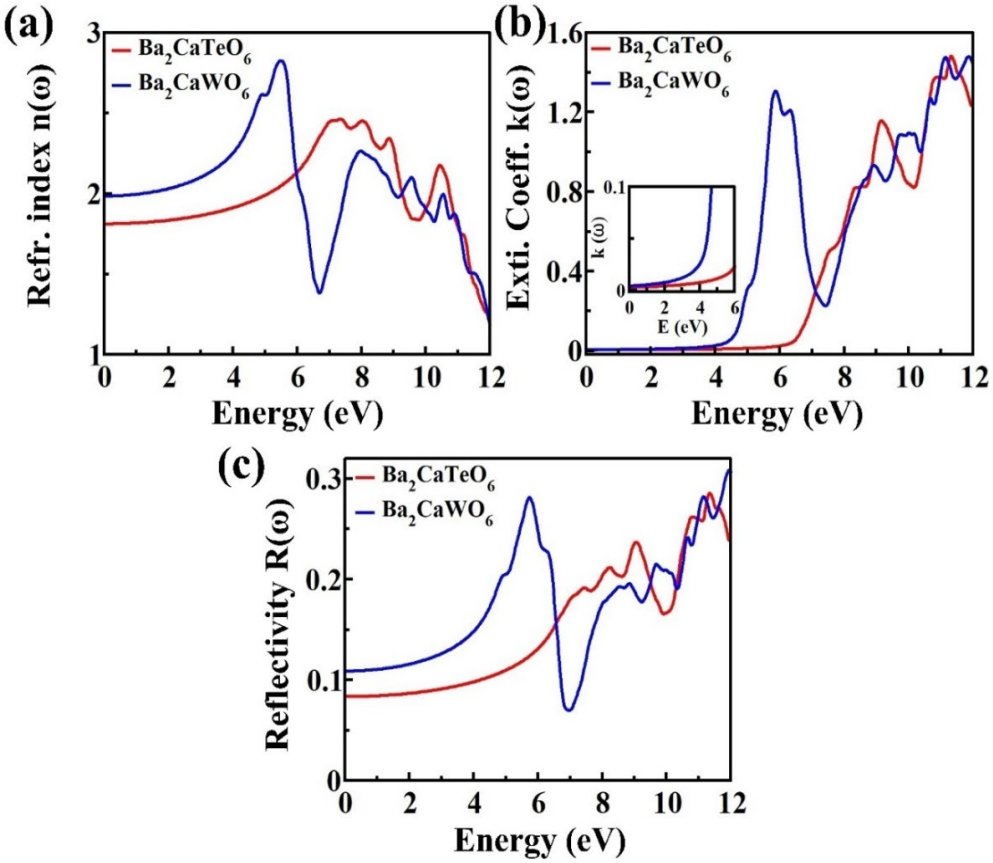

Fig. 7. (a) n(ω)*, (b)* k(ω)*, (c) R(ω) of Ba_2CaXO_6 (X= Te, W).*

For both compounds, absorption begins at zero electron volts and the value of first peak is 4.97 at 9.05 eV for Ba_2CaTeO_6 and 6.41 at 5.73 eV for Ba_2CaWO_6. $\varepsilon_2(\omega)$ for Ba_2CaTeO_6 attained peak value at 10.24 eV, while $\varepsilon_2(\omega)$ for Ba_2CaWO_6 shows peak value at 11.84 eV as indicated in Fig. 6(b).

$$\varepsilon_2(\omega) = \frac{8}{2\pi\omega^2} \sum |P_n\ (x)|^2\ \frac{dS_x}{\nabla\omega_{n\,(k)}} \tag{4}$$

A refractive index n(ω) is also a very useful factor for studying light propagation across the optical medium that finds how fast light goes through it [67]. Its real part can be used for the computation of phase velocity [68]. The determined value of n(0) is 1.825 and 1.98 for Ba_2CaTeO_6 and Ba_2CaWO_6, respectively.

$$n(\omega) = \left(\frac{\left[\varepsilon_1^2\ (\omega) + \varepsilon_2^2(\omega)\right]^{\frac{1}{2}} + \varepsilon_1(\omega)}{2} \right)^{\frac{1}{2}} \tag{5}$$

Ba_2CaTeO_6 has an extreme value of 2.167 at 10.44 eV while Ba_2CaWO_6 has an extreme value of 2.26 at 7.97 eV. n(ω) represents the identical trend to the $\varepsilon_1(\omega)$ (Fig. 7(a)). For Ba_2CaTeO_6 and Ba_2CaWO_6, k(ω) value begins from 0 eV for both compounds and increased to 1.16 at 9.15 eV and 1.306 at 5.85 eV, correspondingly. k(ω) displays peak (see Fig. 7(b)) of 1.48 at 11.3 eV for Ba_2CaTeO_6 and 1.47 at 11.13 eV for Ba_2CaWO_6. The reflectivity R(ω) is vital parameter to understanding a material's optical characteristics [69]. R(ω) shows its static value of 0.48 for Ba_2CaTeO_6 and 0.11 for Ba_2CaWO_6. The top peaks R(ω) value is 0.284 at 11.33 eV (see Fig. 7(c)) for Ba_2CaTeO_6 and 0.308 at 11.94 eV for Ba_2CaWO_6. Table 3 illustrates the computed values of static optical parameters.

$$k(\omega) = \frac{\alpha\lambda}{4\pi} \quad (6)$$

$$R(\omega) = \frac{[n(\omega)-1]^2+k^2(\omega)}{[n(\omega)+1]^2+k^2(\omega)} \quad (7)$$

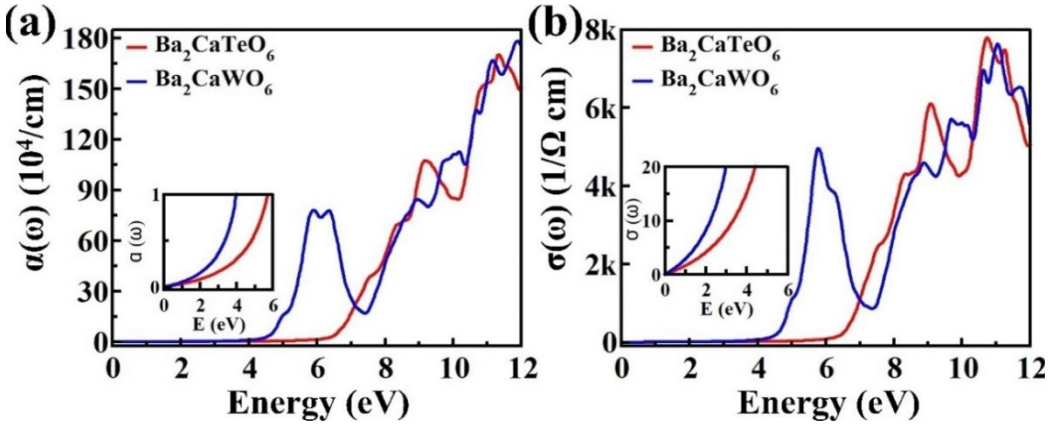

Fig. 8. (a) α(ω), (b) σ(ω) of Ba_2CaXO_6 (X= Te, W).

α(ω) specifies the light absorption per thickness; absorption is higher per thickness if the value of α(ω) is large [70]. The first absorption peak is obtained for Ba_2CaTeO_6 is 107.601 (10^4/cm) at 9.158 eV and for Ba_2CaWO_6 is 77.98 (10^4/cm) at 5.89 eV. Maximum value of α(ω) for Ba_2CaTeO_6 and Ba_2CaWO_6 are 170.28 ×10^4/cm at 11.30 eV and 178.18 ×10^4/cm at 11.87 eV, respectively as indicated in Fig. 8(a). Electrons conduction can be explained by σ(ω) when a suitable frequency of light (photon) collides with the material surface. The first peak of σ(ω) for Ba_2CaTeO_6 is 6074.27 (1/Ωcm) at 9.073 eV and for Ba_2CaWO_6 is 4960.3 (1/Ωcm) at 5.759 eV. The spectrum σ(ω) (see Fig. 8(b)) demonstrates a similar trend of $\varepsilon_2(\omega)$ and k(ω).

$$\alpha = \frac{4\pi k}{\lambda} \quad (8)$$

$$\sigma(\omega) = \frac{\omega}{4\pi}\varepsilon_2(\omega) \quad (9)$$

According to the predicted optical characteristics of Ba_2CaTeO_6 and Ba_2CaWO_6, both DPs are applicable for optoelectronic and photovoltaic devices in UV range.

Table 3. Optical factors for Ba_2CaXO_6 (X= Te, W).

Optical parameters	Ba_2CaTeO_6	Ba_2CaWO_6
$\varepsilon_1(0)$	3.30	3.96
R(0)	0.84	0.11
n(0)	1.825	1.98

3.4. Thermoelectric properties

Squandered heat can be transformed into usable energy to address the worldwide energy issue. The capability of thermoelectric properties (TE) of DPs to effectively convert heat into electricity has caught the attention of scientists [71]. Electrical transport behavior demands a comprehensive understanding of the material's TE features. Double Perovskite oxides have

attracted researchers' interest as TE materials in recent years [72, 73]. Low k/τ, a strong S, and high σ/τ are necessary for efficient TE substance [74].

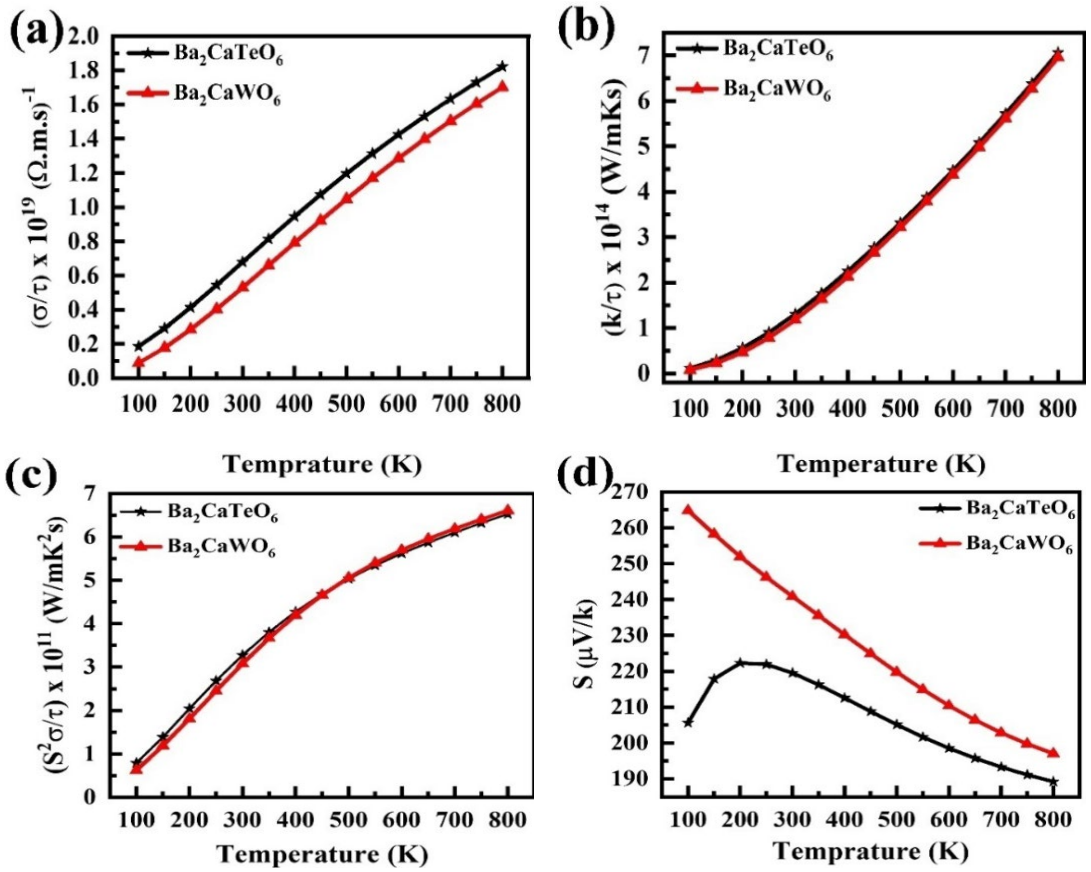

Fig. 9. (a) electrical conductivity, (b) k, (c) PF, (d) S.

At 100 K, calculated σ/τ values for Ba_2CaTeO_6 and Ba_2CaWO_6 are 0.1864 $\times 10^{19}$ and 0.0886 $\times 10^{19}$ $(\Omega m.s)^{-1}$, correspondingly (see Fig. 9(a)), whereas at 800 K, Ba_2CaTeO_6 has the greatest value of 1.8217 $\times 10^{19}$ and Ba_2CaWO_6 has 1.7019 $\times 10^{19}$ $(\Omega m.s)^{-1}$. As temperature rises, the value of σ/τ rises, showing that Ba_2CaTeO_6 and Ba_2CaWO_6 compounds are semiconductors. The response of thermal conductivity (k/τ) for Ba_2CaTeO_6 and Ba_2CaWO_6 between 100 to 800 K is illustrated in Fig. 9(b). The figure depicts the rising of k_e/τ as a function of temperature, comparable to the σ/τ plot's variation.

At 100 K, the lowest k_e/τ value for Ba_2CaTeO_6 and Ba_2CaWO_6 is 0.1140 $\times 10^{14}$(W/mKs), while at 800 K, the highest k_e/τ values are 7.0618 $\times 10^{14}$ (W/mKs) for Ba_2CaTeO_6 and 6.9585 $\times 10^{14}$ (W/mKs) for Ba_2CaWO_6. The power factor (PF), which is a combined effect of S^2 and σ/τ, is crucial parameter in determining an object's efficiency for TE applications. At 100 K, both Ba_2CaXO_6 (X = Te, W) double perovskites have the lower PF value, and increases with temperature.

Both compounds have the same PF (see Fig. 9(c)) value at 500 K, and the uppermost peak of PF for Ba_2CaTeO_6 and Ba_2CaWO_6 is 6.6081 $\times 10^{11}$ and 6.5243 $\times 10^{11}$ (W/mK^2s), respectively at 800 K. Ba_2CaXO_6 (X = Te, W) double perovskite oxide has a similar PF and thermal conductivity (k_e/τ) to Ba_2InTaO_6 [18]. The S for Ba_2CaXO_6 (X = Te, W) materials versus temperature is given in Fig. 9(d) which is representing a decreasing trend along temperature. Moreover, S remains positive within the whole temperature range of 100–800 K.

Figure of merit is used to determine the efficiency of TE material. It is essential for determining the transport features of a compound's [72].

$$ZT = \frac{\sigma S^2}{k} T \quad (10)$$

The value of ZT for Ba_2CaTeO_6 grew linearly with temperature until it reached to 450 K, and obtained its highest estimated value of 0.76. The maximum value of ZT for Ba_2CaWO_6 is 0.79 at 450 K (see Fig.10). Ba_2CaWO_6 double perovskite is well suited for thermoelectric applications due to its high value of PF, S, and ZT (see Table 4).

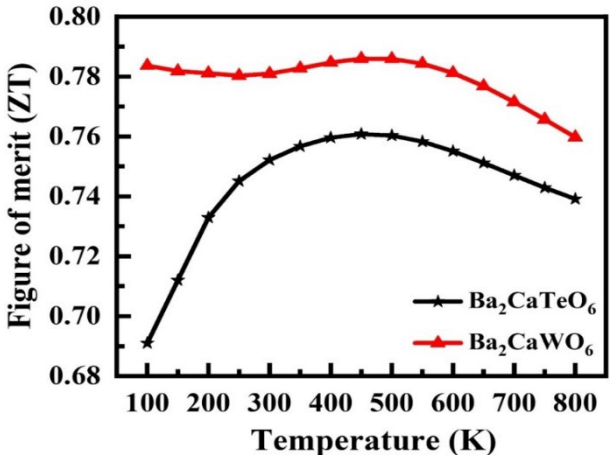

Fig. 10. ZT of Ba_2CaXO_6 (X= Te, W).

Table 4. TE coefficients for Ba_2CaTeO_6 and Ba_2CaWO_6.

Composition	$(\sigma/\tau) \times 10^{19}$ $(\Omega m.s)^{-1}$	$(k/\tau) \times 10^{14}$ (W/mKs)	$PF(S^2\sigma/\tau) \times 10^{11}$ (W/mK^2s)	Seebeck coefficient (S) (μV/k)	ZT
Ba_2CaTeO_6	1.8217 (800 K)	7.0618(800 K)	6.6081(800 K)	189.24(800 K)	0.7607 (450 K)
Ba_2CaWO_6	1.7019(800 K)	6.9585(800 K)	6.5243(800 K)	197.04(800 K)	0.7859(450 K)

4. Conclusions

DFT computations are employed to characterize the optoelectronic, structural, and TE features of Ba_2CaXO_6 (X = Te, W). Both Ba_2CaTeO_6 and Ba_2CaWO_6 compounds demonstrate wide bandgap with E_g of 5.87 eV and 4.20 eV, correspondingly. Thermoelectric transport features such as PF, Seebeck coefficient, ZT, and electrical conductivity are also investigated. ZT values for Ba_2CaTeO_6 and Ba_2CaWO_6 double perovskites are 0.76 and 0.79 at 450 K, correspondingly. Due to its high PF, S, and ZT value, the Ba_2CaXO_6 (X = Te, W) double perovskites are potential contenders for thermoelectric applications. The optical features of Ba_2CaTeO_6 and Ba_2CaWO_6 suggest that both could be used as UV absorbers and sensors.

Acknowledgement

The authors express their gratitude to Princess Nourah bint Abdulrahman University Researchers Supporting Project number (PNURSP2024R81), Princess Nourah bint Abdulrahman University, Riyadh, Saudi Arabia.

References

[1] Wong, M. H., Bierwagen, O., Kaplar, R. J., Umezawa, H., Journal of Materials Research, 1-15 (2021); https://doi.org/10.1557/s43578-021-00458-1
[2] Jishi, R. A., Appleton, R. J., Guzman, D., Applied Physics Letters 117(23), 232102 (2020); https://doi.org/10.1063/5.0027881
[3] Xie, C., Lu, X. T., Tong, X. W., Zhang, Z. X., Liang, F. X., Liang, L., Wu, Y. C., Advanced Functional Materials 29(9), 1806006 (2019); https://doi.org/10.1002/adfm.201806006
[4] Tian, J., Lai, C., Feng, G., Banerjee, D., Li, W. Kar, N.C., International Journal of Sustainable Energy 39(1), 88-100 (2020); https://doi.org/10.1080/14786451.2019.1657866.
[5] Reyren, N., Thiel, S., Caviglia, A. D., Kourkoutis, L. F., Hammerl, G., Richter, C., Schneider, C. W., Kopp, T., Ruitschi, A. S., Jaccard, D., Gabay, M., Muller, D. A., Triscone, J. M., Mannhart, J., *Science 317*(5842), 1196-1199 (2007); http://www.sciencemag.org/content/317/5842/1196.full.html.
[6] Kool, T. W., Muller, K Alex, World Scientific. (2010)
[7] Bugaris, D. E., Hodges, J. P., Huq, A., ZurLoye, H. C., Journal of Solid-State Chemistry 184(8), 2293-2298 (2011); https://doi.org/10.1016/j.jssc.2011.06.015
[8] Lufaso, M. W., Barnes, P. W., Woodward, P. M., Acta Crystallographica Section B: Structural Science 62(3), 397-410 (2006); https://doi.org/10.1107/S010876810600262X
[9] Besbes, A., Djelti, R., Bestani, B., Computational Condensed Matter 19, e00380 (2019); https://doi.org/10.1016/j.cocom.2019.e00380
[10] Siad, A. B., Baira, M., Dahou, F. Z., Bettir, K., Monir, M. E. A., Journal of Solid State Chemistry 302, 122362 (2021); https://doi.org/10.1016/j.jssc.2021.122362
[11] Al-Qaisi, S., Ali, M. A., Alrebdi, T. A., Vu, T. V., Morsi, M., Haq, B. U., Ahmed, R., Mahmood, Q., Tahir, S. A., Materials Chemistry and Physics 275, 125237 (2022); https://doi.org/10.1016/j.matchemphys.2021.125237
[12] Brik, M.G., Journal of Physics and Chemistry of Solids 73(2), 252–256 (2012); https://doi.org/10.1016/j.jpcs.2011.10.034
[13] Elhag, A., Results in Physics 9, 793-805 (2018); https://doi.org/10.1016/j.rinp.2018.03.055
[14] Saad H.-E, M.M., N. Rammeh., Physica B: Condensed Matter 481, 217–223 (2016); https://doi.org/10.1016/j.physb.2015.11.019
[15] Karwasara, H., Bhamu, K. C., Kang, S. G., Kushwaha, A. K., Rai, D. P., Sappati, S., Soni, A., and Sharayia. A., Journal of Alloys and Compounds 893, 162332 (2022); https://doi.org/10.1016/j.jallcom.2021.162332
[16] Ghebouli, B., Ghebouli, M. A., Choutri, H., Fatmi, M., Chihi, T., Louail, L., Bouhemadou. A., Khenata. R., Bin-Omran. S., Khachai, H., Materials Science in Semiconductor Processing. 42, 405-412 (2016); https://doi.org/10.1016/j.mssp.2015.09.026
[17] Haid, S., Bouadjemi, B., Houari, M., Matougui, M., Lantri, T., Bentata, S., Aziz, Z., Solid State Communications 294, 29-35 (2019); https://doi.org/10.1016/j.ssc.2019.03.001
[18] Dar, S. A., Sharma, R., Srivastava, V., Sakalle, U. K., RSC Advances 9(17), 9522-9532 (2019); https://doi.org/10.1039/C9RA00313D
[19] Huma, M., Rashid, M., Mahmood, Q., Algrafy, E., Kattan, N.A., Laref, A., Bhatti, A.S., Materials Science in Semiconductor Processing 121, 105313 (2021); https://doi.org/10.1016/j.mssp.2020.105313.
[20] Mahmood, Q., Ghrib, T., Rached, A., Laref, A., Kamran, M.A., Materials Science in Semiconductor Processing 112, 105009 (2020); https://doi.org/10.1016/j.mssp.2020.105009
[21] Sajjad, M., Mahmood, Q., Singh, N., Larsson, J.A., ACS Applied. Energy Materials 3 (11), 11293–11299 (2020);. https://dx.doi.org/10.1021/acsaem.0c02236.
[22] Murtaza, G., Alshahrani, T., Khalil, R.M.A., Mahmood, Q., Flemban, T.H., Althib, H., Laref, A., Journal of Solid State Chemistry 297, 121988 (2021); https://doi.org/10.1016/j.jssc.2021.121988.
[23] S. Idrissi, R. Khalladi, S. Mtougui, S. Ziti, H. Labrim, I. El Housni, N. El Mekkaoui, L. Bahmad., Physica A: Statistical Mechanics and its Applications 523, 714–722 (2019); https://doi.org/10.1016/j.physa.2019.03.004

[24] Ali, M.A., Dar, S.A., AlObaid, A.A., Al-Muhimeed, T.I., Hegazy, H.H., Nazir, G., Murtaza, G., Journal of Physics and Chemistry of Solid 159, 110258 (2021); https://doi.org/10.1016/j.jpcs.2021.110258
[25] AlObaid, A.A., Rouf, S.A., Al-Muhimeed, T.I., Aljameel, A.I., Bouzgarrou, S., Hegazy, H.H., Alshahrani, T., Naziri, G., AbeerMera, J., Mahmood, Q., Materials Chemistry and Physics 271, 124876 (2021); https://doi.org/10.1016/j.matchemphys.2021.124876.
[26] Umm-e-Hani, Murtaza, G., AlObaid, A.A., Al-Muhimeed, T.I., Al-Qaisi, S., Rehman, A., Hegazy, H.H., Nazir, G., Morsi, M., Mahmood., Q., Journal of solid state chemistry 551, 111322 (2021); https://doi.org/10.1016/j.chemphys.2021.111322.
[27] Asima, A., A. Aldaghfag, S., Zahid, M., Iqbal, J., Yaseen, M., Somaily,H.H., Physica B;Condensed Matter 630, 413694 (2022); https://doi.org/10.1016/j.physb.2022.413694.
[28] Weil, M., Crystallographic Communications 74(7), 1006-1009 (2018); https://doi.org/10.1107/S2056989018009064
[29] Yu, R., Noh, H.M., Moon, B.K., Choi, B.C., Jeong, J.H., Lee, H.S., Jang, K. Yi, S.S., Journal of Luminescence 512, 133-137 (2014); https://doi.org/10.1016/j.jlumin.2014.01.074
[30] Sinha, M., Pearson, T.J., Reeder, T.R., Vivanco, H.K., Freedman, D.E., Phelan, W.A. McQueen, M., Physical Review Materials 3(12), 125002 (2019); https://doi.org/10.1103/PhysRevMaterials.3.125002.
[31] Yaseen, M., Aldaghfag, S. A., and Zahid, M., Materials Science in Semiconductor Processing, 147, 106760 (2022); https://doi.org/10.1016/j.mssp.2022.106760
[32] Regnault, N., Xu, Y., Li, MR., Ma, Da-Shuai., Jovanovic, M., Yazdani, A., Parkin, S.S.P., Felser, C., Schoop, L.M., Ong, N.P., Cava, R.J., Elcoro. L., Song, Z.D., Berneving, B.A., Nature 603, 824–828 (2022); https://doi.org/10.1038/s41586-022-04519-1.
[33] Xueai, Y., Weiwei, F., Xin, Z., Journal of Nanoelectronics and Optoelectronics 15(5), 654-662 (2020); https://doi.org/10.1166/jno.2020.2784.
[34] Andrews, R.L., Heyns, A.M.,Woodward, P.M., Dalton transactions 44(23), 10700-10707 (2015); https://doi.org/10.1039/x0xx00000x.
[35] Sarver-Verhey, T., 28th Joint Propulsion Conference and Exhibit 3204, (2012)
[36] Sreeja, E., Jose, A., George, A., Unnikrishnan, N.V., Joseph, C., Biju, P.R., Infrared Physics and Technology 123, 104184 (2022); https://doi.org/10.1016/j.infrared.2022.104184
[37] Sreeja, E., Vidyadharan, V., Jose, S.K., George, A., Joseph, C., Unnikrishnan, N.V., Biju., Optical Materials 78, 52-62 (2018); https://doi.org/10.1016/j.optmat.2018.02.003
[39] Bode, J.H.G., Van Oosterhout, A.B.,. Journal of Luminescence 10(4), 237-242 (1975); https://doi.org/10.1016/0022-2313(75)90072-1
[40] Zhao, S., Xiang, J., Fang, M.H., Chen, C., Jin, M., Zhang, N., Optical Materials 124, 112052 (2022); https://doi.org/10.1016/j.optmat.2022.112052
[41] Mirinioui, F., Manoun, B., Tamraoui, Y., Lazor, P., Journal of Solid State Chemistry 232, 182-192 (2015)
[42] Trivedi, M., Tallapragada, R.M., Branton, A., Trivedi, D., Nayak, G., Latiyal, O. and Jana, S., Advances in Materials 6(4), 95-100 (2015); https://doi.org/10.11648/j.am.20150406.11.
[43] Tablero, C., Journal of Alloys and Compounds 639, 203-209 (2015); https://doi.org/10.1016/j.jallcom.2015.03.107
[44] Yu, R., Shin, D.S., Jang, K., Guo, Y., Noh, H.M., Moon, B.K., Choi, B.C., Jeong, J.H. Yi, S.S., Spectrochimica Acta Part A: Molecular and Biomolecular Spectroscopy 125, 458-462 (2014); https://doi.org/10.1016/j.saa.2014.01.131
[45] Capece, A.M., Polk, J.E., Shepherd, J.E., Journal of Electron Spectroscopy and Related Phenomena 197, 102-105 (2014); https://doi.org/10.1016/j.elspec.2014.10.001
[46] Popovič, A., Bencze, L., Marsel, J., Lesar, A., Vass-Balthazar, K. and Kaposi, O., Rapid communications in mass spectrometry 7(6), 416-420 (1993); https://doi.org/10.1002/rcm.1290070603
[47] Ruud, J.A. and Bewlay, B.P., Symposium F – High-Temperature Silicides and Refractory Alloys 322, 553-558 (1993)
[48] Sreeja, E., Gopi, S., Vidyadharan, V., Mohan, P.R., Joseph, C., Unnikrishnan, N.V., Biju,P.R., PowderTechnology 323, 445-453 (2018); https://doi.org/10.1016/j.powtec.2017.09.036

[49] Sreeja, E., Gopi, S., Joseph, C., Unnikrishnan, N.V., Biju, P.R., Physica B: Condensed Matter 555, 74-80 (2019); https://doi.org/10.1016/j.physb.2018.11.020
[50] Sreeja, E., Gopi, S., Krishnapriya, T., Unnikrishnan, N.V., Joseph, C., Biju, P.R., Journal of Materials Science: Materials in Electronics 33, 1851-1863 (2022); https://doi.org/10.1007/s10854-021-07384-2.
[51] S. A. Aldaghfag, Nasarullah, A. Aziz, M. Ishfaq, M. Yaseen, Hafsa, S. Jamshaid, Dig. J. Nanomater. Bios. 19, 295-308, (2024); https://doi.org/10.15251/DJNB.2024.191.295
[52] Khan, A. A., Yaseen, M., Laref, A., Murtaza, G., Physica B: Condensed Matter 541, 24-31 (2018); https://doi.org/10.1016/j.physb.2018.04.034
[53] Schwarz, K., Blaha, P., & Madsen, G. K., Computer physics communications 147(1-2), 71-76(2002); https://doi.org/10.1016/S0010-4655(02)00206-0
[54] Aldaghfag, S. A., Aziz, A., Younas, A., Yaseen, M., Murtaza, A., Hegazy, H. H., Journal of Solid State Chemistry 312, 123179 (2022); https://doi.org/10.1016/j.jssc.2022.123179
[55] Yousaf, N., Khan, W., Khan, S. H., Yaseen, M., Laref, A., Murtaza, G., Journal of Alloys and Compounds 737, 637-645 (2018); https://doi.org/10.1016/j.jallcom.2017.12.033
[56] B. Sabir, G. Murtaza, Q. Mahmood, R. Ahmad, K.C. Bhamu, Current Applied Physics 17 (11), 1539–1546 (2017); https://doi.org/10.1016/j.cap.2017.07.010
[57] Perdew, J. P., Ruzsinszky, A., Csonka, G. I., Vydrov, O. A., Scuseria, G. E., Constantin, L. A., Zhou, X., Burke, K., arXiv preprint arXiv:0707.2088. 1-4 (2007); https://arxiv.org/pdf/0707.2088.pdf.
[58] Koller, D., Tran, F., Blaha, P., Physical Review B 85(15), 155109 (2012); https://doi.org/10.1103/PhysRevB.85.155109.
[59] Faizan, M., Murtaza, G., Khan, S. H., Khan, A., Mehmood, A., Khenata, R., Hussain, S., Bulletin of Materials Science 39(6), 1419-1425 (2016); http://doi.org/10.1007/s12034-016-1288-6.
[60] Kazim, M. Z., Ishfaq, M., Aldaghfag, S. A., Yaseen, M., Zahid, M., Nazar, M., and Neffati, R., Journal of Magnetism and Magnetic Materials 560, 169657 (2022), https://doi.org/10.1016/j.jmmm.2022.169657
[61] Li, Z., Yang, M., Park, J. S., Wei, S. H., Berry, J. J., Zhu, K., Chemistry of Materials 28(1), 284-292 (2016); https://doi.org/10.1021/acs.chemmater.5b04107
[62] Al-Qaisi, S., Rai, D. P., Haq, B. U., Ahmed, R., Vu, T. V., Khuili, M. Tahir, S.A., Alhashim, H. H., Materials Chemistry and Physics, 258, 123945 (2021); https://doi.org/10.1016/j.matchemphys.2020.123945
[63] Gassoumi, A., Materials Science in Semiconductor Processing, 50, 14-19 (2016); https://doi.org/10.1016/j.mssp.2016.04.003
[64] Dar, S. A., Srivastava, V., Sakalle, U. K., Parey, V., Pagare, G., Materials Science and Engineering: B 236, 217-224 (2018); https://doi.org/10.1016/j.mseb.2018.12.007
[65] Butt, M.K., Saleem, S., Al-Harbi, F.F, Atta, S., Ishfaq, M., Al-Juman, F.S., Journal of Chalcogenide Letters 20, 459-467 (2023); https://doi.org/10.15251/CL.2023.207.459
[66] A.M. Shawahni, M.S. Abu-Jafar, R.T. Jaradat, T. Ouahrani, R. Khenata, A.A. Mousa, K.F. Ilaiwi., Materials 11 (10), 2057 (2018); https://doi.org/10.3390/ma11102057
[67] A.G. El Hachimi, M.L. Ould, NE, A. El Yousfi, A. Benyoussef, A. El Kenz., Optical and Quantum Electronics 53 (2), 95 (2021)
[68] Sheikh, M. S., Sakhya, A. P., Maity, R., Dutta, A., Sinha, T. P., Solar Energy Materials and Solar Cells 193, 206-213 (2019); https://doi.org/10.1016/j.solmat.2019.01.015
[69] Saeed, Y., Amin, B., Khalil, H., Rehman, F., Ali, H., Khan, M. I., Mahmood, A., Shafiq, M., RSC Advances 10(30), 17444-17451 (2020); http://doi.org/10.1039/d0ra01764g.
[70] Hassan, M., Arshad, I., Mahmood, Q., Semiconductor Science and Technology 32(11), 115002 (2017); https://doi.org/10.1088/1361-6641/aa8afe.
[71] Yaseen, M., Dilawar, M., Ambreen, H., Bibi, S., Rehman, S. U., Shahid, U., Butt. M. K., Ghaffar, A., Murtaza, A., Bulletin of Materials Science 43(1), 1-8 (2020); https://doi.org/10.1007/s12034-020-2078-8.
[72] Hanif, A., Aldaghfag, S. A., Aziz, A., Yaseen, M., Murtaza, A., International Journal of Energy Research 46(8), 10633-10643 (2022); https://doi.org/10.1002/er.7862
[73] Haid, S., Benstaali, W., Abbad, A., Bouadjemi, B., Bentata, S., Aziz, Z., Materials Science and Engineering: B 245,68-74 (2019); https://doi.org/10.1016/j.mseb.2019.05.013

[74] Dar, S. A., Srivastava, V., Sakalle, U. K., Journal of Magnetism and Magnetic Materials 484, 298-306 (2019); https://doi.org/10.1016/j.jmmm.2019.04.048.
[75] Madsen, G. K., Singh, D. J., Computer Physics Communications 175(1), 67-71 (2006); https://doi.org/10.1016/j.cpc.2006.03.007